

The high-k poloidal scattering system for NSTX-U

R. Barchfeld, C. W. Domier, Y. Ren, R. Ellis, P. Riemenschneider, N. Allen, R. Kaita, B. Stratton, J. Dannenberg, Y. Zhu, and N. C. Luhmann

Citation: [Review of Scientific Instruments](#) **89**, 10C114 (2018); doi: 10.1063/1.5035410

View online: <https://doi.org/10.1063/1.5035410>

View Table of Contents: <http://aip.scitation.org/toc/rsi/89/10>

Published by the [American Institute of Physics](#)

Articles you may be interested in

[Zeeman splitting measurements of magnetic fields in iodine plasma](#)

[Review of Scientific Instruments](#) **89**, 10C113 (2018); 10.1063/1.5038641

[Liquid crystal polymer receiver modules for electron cyclotron emission imaging on the DIII-D tokamak](#)

[Review of Scientific Instruments](#) **89**, 10H120 (2018); 10.1063/1.5035373

[A multi-species powder dropper for magnetic fusion applications](#)

[Review of Scientific Instruments](#) **89**, 10K121 (2018); 10.1063/1.5039345

[Characterization and calibration of the Thomson scattering diagnostic suite for the C-2W field-reversed configuration experiment](#)

[Review of Scientific Instruments](#) **89**, 10C120 (2018); 10.1063/1.5037101

[The surface eroding thermocouple for fast heat flux measurement in DIII-D](#)

[Review of Scientific Instruments](#) **89**, 10J122 (2018); 10.1063/1.5038677

[Simulation, design, and first test of a multi-energy soft x-ray \(SXR\) pinhole camera in the Madison Symmetric Torus \(MST\)](#)

[Review of Scientific Instruments](#) **89**, 10G116 (2018); 10.1063/1.5038798



PFEIFFER VACUUM

VACUUM SOLUTIONS FROM A SINGLE SOURCE

Pfeiffer Vacuum stands for innovative and custom vacuum solutions worldwide, technological perfection, competent advice and reliable service.

[Learn more!](#)

The high- k poloidal scattering system for NSTX-U

R. Barchfeld,¹ C. W. Domier,^{1,a)} Y. Ren,² R. Ellis,² P. Riemenschneider,¹ N. Allen,² R. Kaita,² B. Stratton,² J. Dannenberg,¹ Y. Zhu,¹ and N. C. Luhmann, Jr.¹

¹Department of Electrical and Computer Engineering, University of California, Davis, California 95616, USA

²Princeton Plasma Physics Laboratory, Princeton, New Jersey 08543, USA

(Presented 19 April 2018; received 15 April 2018; accepted 25 June 2018; published online 8 October 2018)

An 8-channel, high- k poloidal far-infrared (FIR) scattering system is under development for the National Spherical Torus eXperiment Upgrade (NSTX-U). The 693 GHz poloidal scattering system replaces a 5-channel, 280 GHz high- k toroidal scattering system to study high- k electron density fluctuations on NSTX-U. The FIR probe beam launched from Bay G is aimed toward Bay L, where large aperture optics collect radiation at 8 simultaneous scattering angles ranging from 2° to 15° . The reduced wavelength in the poloidal system results in less refraction, and coupled with a new poloidal scattering geometry, extends measurement of poloidal wavenumbers from the previous limit of 7 cm^{-1} up to $>40\text{ cm}^{-1}$. Steerable launch optics coupled with receiver optics that can be remotely translated in 5 axes allow the scattering volume to be placed from $r/a = 0.1$ out to the pedestal region ($r/a \sim 0.99$) and allow for both upward and downward scattering to cover different regions of the 2D fluctuation spectrum. *Published by AIP Publishing.* <https://doi.org/10.1063/1.5035410>

I. INTRODUCTION

In the National Spherical Torus eXperiment (NSTX), electron-scale turbulence was successfully measured using a 5-channel toroidal collective scattering system.¹ The probe beam was launched tangentially into the plasma; the scattering system primarily measured radial wavenumber, k_r , components and finite but smaller poloidal wavenumber, k_θ , that satisfies the Bragg condition $k = 2k_i \sin(\theta_s/2)$, where k is the fluctuation wavenumber, k_i is the incident wavenumber, and θ_s is the scattering angle. By measuring the scattered power and frequency shift at five distinct scattering angles, the turbulence wavenumber spectra were obtained at five different points in the 2D plane of k_r and k_θ .²

Available ports and spatial constraints on NSTX permitted the installation of this toroidal scattering system. However, a strong limitation of this system is that it was unable to resolve the dominant spectral components of electron transport gradient (ETG) turbulence³ which are typically the modes with large k_θ and small k_r .⁴ New port window designs on National Spherical Torus eXperiment Upgrade (NSTX-U)⁵ allowed for the development of a poloidal high- k_θ scattering system to target predicted ETG modes with an improved k_θ range and resolution. In the poloidal scattering scheme illustrated in Fig. 1, a probe beam drawn in blue illuminates a flux surface below the plasma mid-plane with scattered beams going upward through the exit window. With the probe beam propagating upward above the mid-plane, the scattered beams drawn in red propagate downward through the window.

Note: Paper published as part of the Proceedings of the 22nd Topical Conference on High-Temperature Plasma Diagnostics, San Diego, California, April 2018.

^{a)}Author to whom correspondence should be addressed: cwdomier@ucdavis.edu.

Details regarding the probe beam and launch optics are presented in Sec. II, the scattering receiver and receiver optics in Sec. III, a retractable wedge that simplifies the receiver optics in Sec. IV, and the mechanical receiver carriage in Sec. V. The scattering electronics are described in Sec. VI, followed by a brief summary in Sec. VII.

II. PROBE BEAM AND LAUNCH OPTICS

An Edinburgh Instruments PL-6 CO₂ laser⁶ optically pumps a formic acid, far-infrared (FIR) laser to generate a $>80\text{ mW}$ FIR beam at 693 GHz ($432\text{ }\mu\text{m}$).⁷ For use as a pump laser for the formic acid laser, the PL-6 is tuned to the 9R20 ($9.27\text{ }\mu\text{m}$) spectral line, where it can produce up to 170 W CW. The lasers are mounted on a 3-level laser table (see Fig. 2) housed in a laser cage area outside the NSTX-U

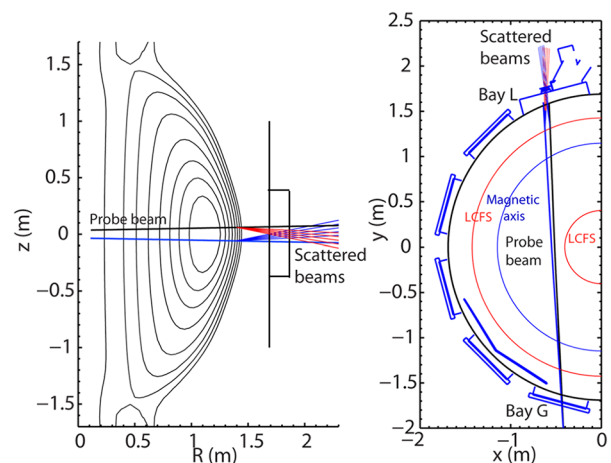


FIG. 1. Side (left) and top (right) view illustrations of the two poloidal scattering schemes (upward and downward scattering) on NSTX-U.

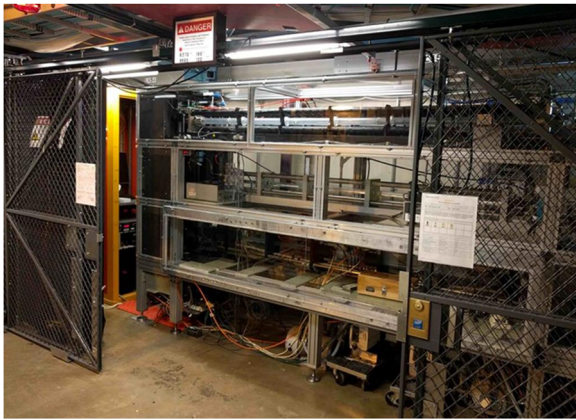


FIG. 2. Photograph of the laser cage area, showing the FIRETIP lasers installed with space reserved for the high- k_0 lasers.

test cell, which is shared with 4 additional lasers (one CO₂ and 3 FIR) that are part of the Far-infrared Tangential Interferometer/Polarimeter (FIRETIP) system.⁸ The lower level of the laser tower houses the CO₂ pump lasers for both the high- k_0 scattering and FIRETIP systems, and the middle level houses the high- k_0 scattering FIR laser and one of the FIRETIP FIR lasers, while the top level houses the remaining two FIRETIP FIR lasers.

The linearly polarized FIR beam is transported from the laser cage area, through a 4-foot-thick concrete wall that separates the laser cage area from the NSTX-U test cell, to the vacuum vessel via ~20 m of low loss, corrugated metallic waveguide (see Fig. 3) that is back-filled with nitrogen to minimize absorption loss. Using equations from Ref. 9 for the linearly polarized HE₁₁ hybrid mode that is excited within the waveguide, a set of corrugation parameters (see Fig. 4) were determined by striking a balance between low attenuation and ease of machinability. The theoretical loss at

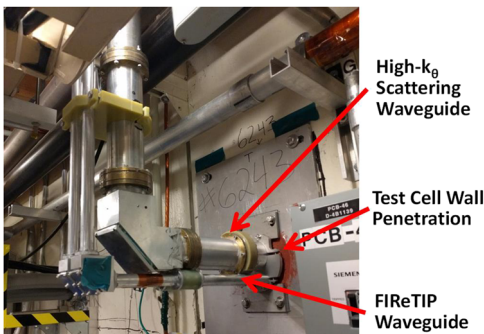


FIG. 3. Photograph of the high- k and FIRETIP waveguide runs at the exit of the NSTX-U test cell wall.

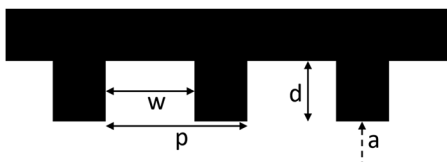


FIG. 4. Corrugated waveguide dimensions: $a = 31.5$ mm, $d = 127$ μm , $w = 188$ μm , and $p = 300$ μm .

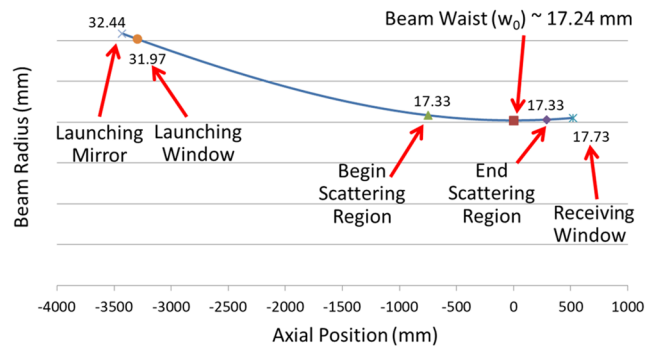


FIG. 5. Simulated Gaussian beam radius of the launch beam, from the Bay G launching mirror to the Bay L receiving window.

693 GHz is calculated to be on the order of 2×10^{-5} dB/m; laboratory measurements indicate that the actual loss is likely to be ~0.1 dB/m for a total loss of ~2 dB over the ~20 m waveguide path length.

Before the FIR beam passes through the launch window on Bay G, it will traverse the launch optics assembly to steer and shape the beam. The probe beam then enters the vacuum vessel through a z-cut crystal quartz window (the optical axis of the crystal is perpendicular to the window surfaces to minimize transmission loss); the remote-controlled mirror immediately next to the entrance window can steer the beam by $\pm 2.2^\circ$ vertically and $\pm 1.0^\circ$ horizontally. The shaping optics generate a 17-18 mm radius Gaussian beam waist in the plasma ~520 cm short of the Bay L exit window (see Fig. 5), which helps to minimize the scattering volume of the high- k_0 receiver. At the

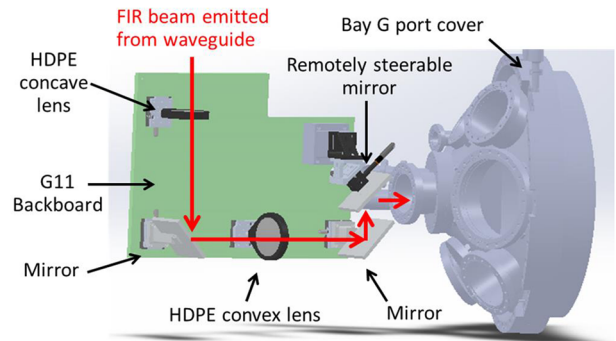


FIG. 6. Schematic layout of the high- k_0 launch optics positioned next to the Bay G port cover on NSTX-U.



FIG. 7. Photograph of the high- k_0 launch optics assembly, mounted on a G11 backboard, with Lexan paneling removed.

extreme ends of the scattering region, the probe beam remains reasonably collimated; the minimal divergence therefore still provides good scattering properties. The launch optics assembly is shown in Figs. 6 and 7 and is supported by a cantilever truss arrangement.

III. SCATTERING RECEIVER AND RECEIVER OPTICS

Density fluctuations along the path of the probe beam will cause the beam to forward scatter and be collected by receiver optics placed outside of Bay L. The Bay L window is made of Corning 7979 IR-grade fused silica, whose hydroxyl ion (OH^-) concentration is <1 ppm to minimize absorption within the 0.625-inch-thick window; the window attenuation at 693 GHz is calculated to be roughly 3 dB.

The heart of the High- k scattering receiver is a 4-element subharmonic mixer (SHM) array, fabricated by Virginia Diodes, Inc. and shown in Fig. 8. The array is pumped by a high power multiplier that delivers >600 mW at ~ 115.5 GHz, which is then tripled internally to ~ 346 GHz. A pair of SHM arrays will be placed end-to-end to achieve an 8-element receiver with a channel-to-channel spacing of 30.0 mm. The RF input to each mixer is via a small diagonal horn (2 mm on each side), in front of which is placed a small collimating lens to form a Gaussian beam waist of roughly 7.5 mm radius at the surface of the small lens. Each of the small lenses can be individually adjusted in two axes using miniature, manual dovetail stages with several millimeters of adjustability in each plane.

The receiver optics consist of two high density polyethylene (HDPE) lenses: a large collecting lens and a smaller meniscus lens. A Gaussian beam propagation simulation is provided in Fig. 9, showing how the imaging optics focus all 8 channels onto the same scattering volume but with a different scattering angle for each. This is key to obtaining a localized scattering volume, which we can define as the intersection of the individual receiver beams with that of the probe beam. As the receiver beams are tilted toroidally with respect to the probe beam, we therefore obtain a compact scattering volume by translating/rotating the receiver optics such that the point at which the 8 receiver beams meet is placed at the desired point along the probe beam. Forward scattering that occurs at other points along the probe beam will thus not be imaged onto the receiver.

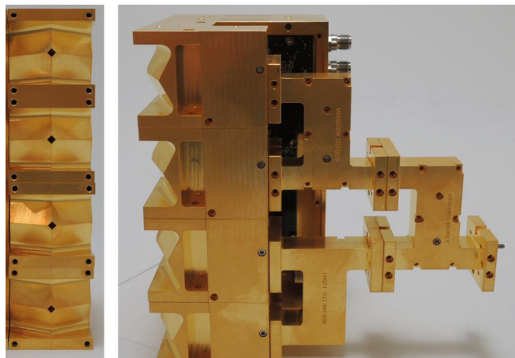


FIG. 8. Photographs of the 692 GHz 4-element subharmonic mixer (SHM) array developed by VDI. Photos.

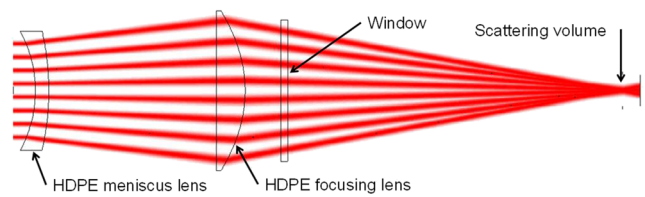


FIG. 9. Gaussian beam simulation of the High- k_0 receiver optics, from the array (far left) to the scattering volume (far right).

The optics are fixed to the SHM arrays, thereby maintaining a tight focus to the scattering volume at all times. The entire optics assembly must therefore be rotated and translated as a single unit to place the scattering volume in the desired region of the plasma for a given physics study. Here, the scattering volume can be positioned radially from $r/a \sim 0.1$ to the plasma edge (a radial distance of ~ 50 cm) and as much as ± 15 cm off the plasma mid-plane.

IV. RETRACTABLE 2-PART DIELECTRIC WEDGE

The receiver optics requires poloidal steering from -4° (aimed downward for upward scattering) to $+4^\circ$ (aimed upward for downward scattering). Immediately above the scattering diagnostic, however, is another diagnostic: the Fusion Products detector.¹⁰ This is attached to a port above and to the left of the exit window on Bay L. As the receiver is tilted toroidally to the Bay L port cover by roughly 14° , this prevents the receiver optics from vertically translating above the plasma mid-plane as required for upward scattering, as illustrated in Fig. 10.

This problem is alleviated by the use of a dielectric wedge, which can poloidally shift the location of the scattering volume when inserted. This is illustrated in Fig. 11, where an HDPE wedge (each side tilted by 3.3°) inserted just outside the vacuum window is seen to shift the scattering volume downwards by 4.0° . On NSTX-U, this will be implemented as a retractable 2-part dielectric wedge (see Fig. 12), where the thickness of each 310 mm tall HDPE wedge varies from a minimum of 4.1 mm at the top of each wedge to a maximum of 22.0 mm at the bottom. To achieve an upward scattering tilt of an angle θ_0 between 0.0° and 4.0° , the wedges are inserted and the receiver carriage are adjusted for an angle of $4.0^\circ - \theta_0$. When not needed, the wedge opens up

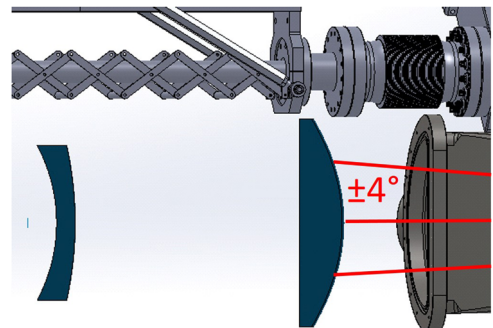


FIG. 10. Side view of the High- k_0 receiver optics placed next to the Bay L port cover, showing the Fusion Products detector placed above the High- k_0 receiver.

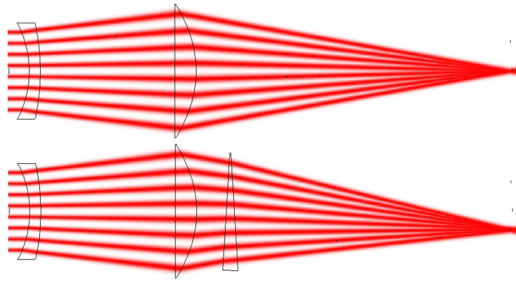


FIG. 11. Gaussian beam simulations taken without (top) and with (bottom) a dielectric wedge inserted into the beam, showing how the scattering volume can be poloidally steered by 4.0° .

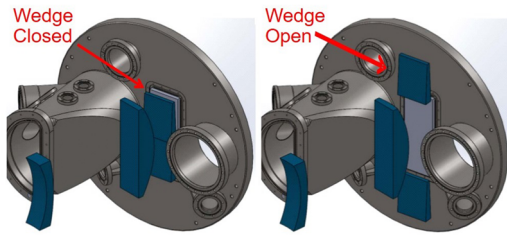


FIG. 12. Schematic layout showing how a two-part HDPE wedge, mounted on the Bay L port cover, can be opened and closed to poloidally steer the scattered beams.

to sit out of the way above and below the Bay L scattering window.

V. RECEIVER CARRIAGE

The use of a retractable dielectric wedge significantly reduces the overall range of travel that the receiver needs to accommodate: a rotation range of 0° to -4° poloidally and $\pm 2^\circ$ toroidally, a radial travel of 500 mm, a toroidal travel of 76 mm, and a vertical travel of 76 mm. The position of the receiving optics is coordinated with the probe beam line to choose the location of the scattering volume, which can be repositioned remotely between plasma discharges. A five-axis (X, Y, Z, poloidal, and toroidal) receiver carriage has been designed to perform this task and is shown schematically in Fig. 13.

Each axis is positioned individually under LabVIEW control; simultaneous motion is not required. A JY Instrument J02DX100S rotation stage is employed for horizontal receiver rotation, while poloidal rotation is achieved using a low profile

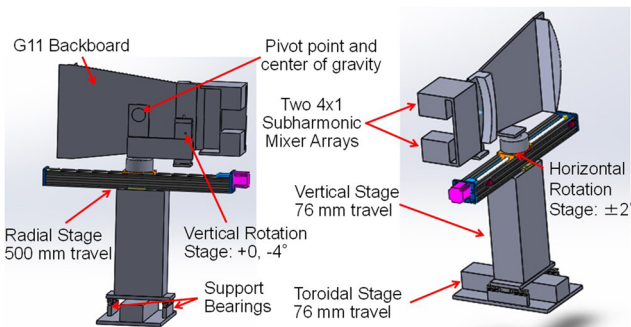


FIG. 13. Schematic diagram of the High- k_0 receiver mounted on a five-axis receiver carriage.

linear stage to act on a level arm about a pivot point near the center of gravity. Immediately below, the horizontal rotation stage is a Velmex 20 inch BiSlide for radial positioning. A heavy duty lab jack (JY Instrument J03DS100S) allows for a 100 mm vertical travel range. Finally, a Velmex 5 inch BiSlide provides toroidal positioning, with support bearings on either side to carry the load and prevent binding when the receiver carriage is positioned at either of the radial extremes.

VI. SCATTERING ELECTRONICS

A double down-conversion scheme is employed to convert the scattered FIR signals to low intermediate frequencies that are subsequently digitized. This is shown schematically in Fig. 14. The first down-conversion step takes place in the SHM receiver array that is pumped by a 14.418 GHz microwave local oscillator (LO) signal that is multiplied by 24x to 346.03 GHz. This results in an unscattered 692.95 GHz signal being downconverted to $692.95 - 2 \times 346.03 \approx 0.89$ GHz.

The scattered beams are up- or down-shifted by the frequency of electron density fluctuations in the scattering region as well as Doppler-shifted by the poloidal and toroidal rotation of the plasma in the scattering region. In the case of NSTX-U, this Doppler shift can be as high as 15-20 MHz at the plasma edge and can greatly exceed the natural mode fluctuation frequency which for ETG turbulence is $\lesssim 5$ MHz. An up-shifted 15 MHz scattering signal would thus appear at $890 + 15 = 905$ MHz, while a similarly down-shifted 15 MHz scattering signal would appear at $890 - 15 = 875$ MHz.

A small portion of the 692.95 GHz beam from the corrugated waveguide line running from the FIR laser to the Bay G launch optics is split off, using a miter tee in which the internal mirror has been replaced by a dielectric beam splitter. This is fed to the Farran WHMB-2.2 harmonic mixer within the reference mixer box, that is pumped by the same 14.418 GHz LO signal as shown in Fig. 14. Mixing with the 48th harmonic of

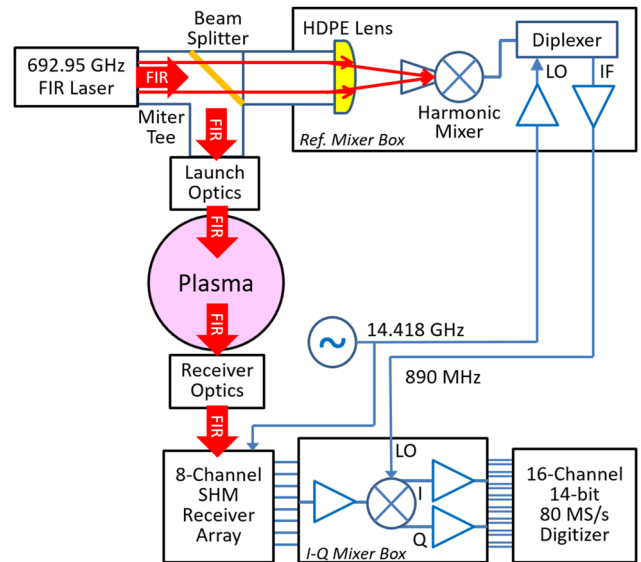


FIG. 14. Schematic diagram of the scattering electronics.

the LO signal, the harmonic mixer generates an ~ 0.89 GHz reference signal (separated from the LO signal using a coaxial microwave diplexer) which is transported via the coaxial cable to the I-Q mixer box where the second down-conversion step takes place.

Inside the I-Q mixer box are 8 parallel circuits, each consisting of a low noise amplifier and an in-phase/quadrature (I/Q) demodulator followed by a pair of wide bandwidth (≥ 40 MHz) video amplifiers. Two output in-phase and quadrature signals, $I(t)$ and $Q(t)$, are generated for each scattering channel. The resultant $2 \times 8 = 16$ output signals will be digitized by D-Tacq ACQ480-8-LFP 14-bit analog input modules running at an 80 MSPS/channel.

VII. SUMMARY

An 8-channel, 693 GHz, poloidal High- k_θ scattering system is under development for NSTX-U. The diagnostic system is primarily configured for poloidal scattering, sampling the scattered fluctuation spectrum at 8 simultaneous scattering angles corresponding to poloidal wavenumbers up to $>40 \text{ cm}^{-1}$. A five-axis receiver carriage allows the scattering volume to be positioned anywhere from the magnetic axis to the outboard edge ($r/a \sim 0.99$).

ACKNOWLEDGMENTS

This work is supported by the United States Department of Energy under Contract Nos. DE-FG02-99ER54518 and DEAC02-09CH11466.

- ¹D. R. Smith, E. Mazzucato, W. Lee, H. K. Park, C. W. Domier, and N. C. Luhmann, Jr., *Rev. Sci. Instrum.* **79**, 123501 (2008).
- ²Y. Ren, W. Guttenfelder, S. M. Kaye, R. E. M. Bell, C. W. Domier, B. P. LeBlanc, K. C. Lee, M. Podesta, D. R. Smith, and H. Yuh, *Nucl. Fusion* **53**, 083007 (2013).
- ³Y. Ren, E. Belova, N. Gorelenkov, W. Guttenfelder, S. M. Kaye, E. Mazzucato, J. L. Peterson, D. R. Smith, D. Stutman, K. Tritz, W. X. Wang, H. Yuh, R. E. Bell, C. W. Domier, and B. P. LeBlanc, *Nucl. Fusion* **57**, 072002 (2017).
- ⁴J. E. Menard *et al.*, *Nucl. Fusion* **52**, 083015 (2012).
- ⁵W. Guttenfelder and J. Candy, *Phys. Plasmas* **18**, 022506 (2011).
- ⁶Edinburgh Instruments, Inc., The PL Series Infrared Lasers Technical Specs, 2011, <https://www.edinst.com/wp-content/uploads/2015/09/PL-Series-technical-specs.pdf>.
- ⁷G. Dodel, *Infrared Phys. Technol.* **40**, 127 (1999).
- ⁸E. R. Scott, R. Barchfeld, P. Riemenschneider, C. W. Domier, C. M. Muscatello, M. Sohrabi, R. Kaita, Y. Ren, and N. C. Luhmann, Jr., *Rev. Sci. Instrum.* **87**, 11E114 (2016).
- ⁹E. A. Nanni, S. K. Jawla, M. A. Shapiro, P. P. Woskov, and R. J. Temkin, *J. Infrared, Millimeter, Terahertz Waves* **33**, 695 (2012).
- ¹⁰R. V. Perez, "A charged fusion product diagnostic for a spherical tokamak," Ph.D. dissertation (Florida International University, 2015), <http://digitalcommons.fiu.edu/etd/2233/>.